

Notes

The Zirconocene Dihydride–Alane Adducts
 $[(\text{Cp}')_2\text{ZrH}(\mu\text{-H})_2]_3\text{Al}$ and
 $[(\text{Cp}')_2\text{ZrH}(\mu\text{-H})_2]_2\text{AlH}$ ($\text{Cp}' = \text{Me}_3\text{SiC}_5\text{H}_4$)

Nola Etkin[†] and Douglas W. Stephan*

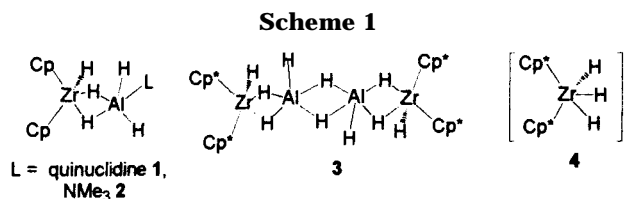
*Department of Chemistry and Biochemistry, University of Windsor,
Windsor, Ontario, Canada N9B 3P4*

Received September 29, 1997

Summary: The reaction of $(\text{Me}_3\text{SiC}_5\text{H}_4)_2\text{ZrCl}_2$ with excess LiAlH_4 affords the product **5**. The structural characterization of **5** reveals two types of aggregation of the $(\text{Me}_3\text{SiC}_5\text{H}_4)_2\text{ZrH}_2$ and AlH_3 fragments formulated as $[(\text{Me}_3\text{SiC}_5\text{H}_4)_2\text{ZrH}(\mu\text{-H})_2]_3\text{Al}$ and $[(\text{Me}_3\text{SiC}_5\text{H}_4)_2\text{ZrH}(\mu\text{-H})_2]_2\text{AlH}$. In this Zr_3Al aggregate, three zirconocene units form two hydrogen-atom bridges, each to a central aluminum atom, generating a pseudo-octahedral environment about the aluminum center. In each of the $\text{Zr}_2\text{-Al}$ aggregates, two zirconocene fragments are bridged to a central aluminum center by two hydride atoms, yielding a distorted square-based pyramid geometry about Al. These results are presented and the implications considered.

Introduction

The interactions of group IV metal complexes with aluminum reagents is the foundation of a number of catalytic processes.¹ Despite this, studies of group IV-aluminum hydrides have been limited to date.² In a very recent paper, Raston et al.³ have described structural studies of the first “purely hydridic” Zr–Al species $\text{Cp}_2\text{-ZrH}(\mu\text{-H}_2)\text{AlH}_2(\text{L})$ (L = quinuclidine (**1**), NMe_3 (**2**)). In these compounds, two hydrogen atoms bridge Zr and Al while the N-based donor coordinates to the Lewis acidic Al center. In very recent work, we have reported⁴ that the species $[\text{Cp}^*_2\text{ZrH}(\mu\text{-H}_2)\text{AlH}_2]_2$ (**3**) reacts rapidly with BuLi to give the first early transition metal-based hydride anion, $[\text{Cp}^*_2\text{ZrH}_3]^-$ (**4**). In the solid-state structural study of **3**, hydrogen atoms bridge the $\text{ZrAl}_2\text{-Zr}$ array. While the $\text{Zr}(\mu\text{-H}_2)\text{Al}$ bridging is similar to that observed in **1** or **2**, the absence of additional base leads to $\text{Al}(\mu\text{-H}_2)\text{Al}$ bridging and thus the extended array. A similarly extended hydrogen-bridged array is



presumed for the Ti(III) species $[\text{Cp}^*_2\text{Ti}(\mu\text{-H}_2)\text{AlH}_2]_2$ ⁵ and $[\text{Cp}_2\text{Ti}(\mu\text{-H}_2)\text{Al}(\mu\text{-H}_2)(\text{C}_5\text{H}_4)\text{TiCp}(\mu\text{-H}_2)]_2$.⁶ In this report, we describe the product of the reaction of $(\text{Cp}')_2\text{-ZrCl}_2$ ($\text{Cp}' = \text{Me}_3\text{SiC}_5\text{H}_4$) with LiAlH_4 , **5**. The structural characterization of **5** reveals two novel types of aggregation of the $(\text{Cp}')_2\text{ZrH}_2$ and AlH_3 fragments. These results are presented and the implications considered.

Experimental Section

General Data. All preparations were performed under an atmosphere of dry, O_2 -free N_2 employing either Schlenk-line techniques or an Innovative Technology inert atmosphere glovebox. Solvents were reagent grade, distilled from the appropriate drying agents under N_2 , and degassed by the freeze–thaw method at least 3 times prior to use. All organic reagents were purified by conventional methods. ^1H and $^{13}\text{C}\{^1\text{H}\}$ NMR spectra were recorded on Bruker Avance 300 and 500 MHz spectrometers. Trace amounts of protonated solvents were used as references, and chemical shifts are reported relative to SiMe_4 . Combustion analyses were performed by Galbraith Laboratories, Inc., (Knoxville, TN) or Schwarzkopf Laboratories (Woodside, NY).

Synthesis of 5. To a suspension of $(\text{Cp}')_2\text{ZrCl}_2$ (534 mg, 1.22 mmol) in ether (5 mL) was added LiAlH_4 (100 mg, 264 mmol) as a suspension in ether (4 mL). The mixture was stirred overnight and then filtered, and the solvent was removed in vacuo. The temperature-sensitive residue was recrystallized from ether/pentane at -35°C to give colorless crystals of **5** in 90% yield. ^1H NMR (C_6D_6 , 25°C) δ : 5.96 (s, 14H), 5.54 (s, 14H), 5.37 (s, 14H), 5.21 (s, 14H), 2.06 (br s, 7H), 0.35 (br s, 56H), 0.33 (s, 70H), -2.05 (br s, 7H), -2.57 (br s, 7H). $^{13}\text{C}\{^1\text{H}\}$ NMR (C_6D_6 , 25°C) δ : 112.3, 106.2, 105.6, 104.6, 104.5, 103.2, 1.2. Anal. Calcd for $\text{C}_{112}\text{H}_{205}\text{Al}_3\text{Si}_{14}\text{Zr}_7$ (**5**): C, 58.90; H, 8.99; Found: C, 58.18; H, 8.97.

(5) Belsky, V. K.; Sizov, A. I.; Bulychev, B. M.; Soloveichik, G. I. *J. Organomet. Chem.* **1985**, *280*, 67.

(6) Lobkovskii, E. B.; Solveichik, G. I.; Sizov, A. I.; Bulychev, B. M. *J. Organomet. Chem.* **1985**, *280*, 53.

[†] Current address: Department of Chemistry, University of Prince Edward Island, 550 University Ave., Charlottetown, Prince Edward Island, Canada, C1A 4P3.

(1) Cardin, D. J.; Lappert, M. F.; Raston, C. L. *Chemistry of Organometallic and Hafnium Compounds*; Ellis Horwood: Chichester, U.K., 1986.

(2) Camalt, C. J.; Norman, N. C.; Clarkson, L. C. *Comprehensive Organometallic Chemistry II*; Abel, E. W., Stone, F. G. A. S., Wilkinson, G., Eds.; Pergamon Press: Oxford, U.K., 1995; Vol. 1, p 545.

(3) Khan, K.; Raston, C. L.; McGrady, J. E.; Skelton, B. W.; White, A. H. *Organometallics* **1997**, *16*, 3252.

(4) Etkin, N.; Hoskin, A. J.; Stephan, D. W. *J. Am. Chem. Soc.* **1997**, *118*, 11420.

Table 1. Crystallographic Data¹

	5
formula	C ₁₁₂ H ₁₉₁ Al ₃ Si ₁₄ Zr ₇
fw	2664.50
a, Å	12.8341(2)
b, Å	22.8541(3)
c, Å	48.4296(2)
β, deg	93.585(1)
V, Å ³	14177.2(2)
space group	P2 ₁ /a
D(calcd), g cm ⁻³	1.248
Z	4
μ, mm ⁻¹	0.670
no of data collected	33 725
no. of indep data	14 851
2θ index ranges, deg	4.5–57
no. of data with F _o ² > 2σ(F _o ²)	8272
no. of variables	1294
R1 (%) (obsd data)	0.1108
wR2 (%) (all data)	0.2918
gof (all data)	1.009

X-ray Data Collection and Reduction. X-ray quality crystals of **5** were obtained directly from the preparation described above. The crystals were manipulated and mounted in capillaries in a glovebox, thus maintaining a dry, O₂-free environment for each crystal. Diffraction experiments were performed on a Siemens SMART System CCD diffractometer collecting a hemisphere of data in 1329 frames with 10 s exposure times. Crystal data are summarized in Table 1. The observed extinctions were consistent with the space group. The data set was collected (4.5° < 2θ < 57.0°). A measure of decay was obtained by re-collecting the first 50 frames of the data set. The intensities of the reflections within these frames showed no statistically significant change over the duration of the data collections. The data were processed using the SAINT and XPREP processing package. An empirical absorption correction based on redundant data was applied. Subsequent solution and refinement was performed using the SHELXTL solution package operating on a SGI Challenge mainframe computer with remote X-terminals or a PC employing X-emulation.

Structure Solution and Refinement. Non-hydrogen atomic scattering factors were taken from the literature tabulations.⁷ The Zr atom positions were determined using the SHELXTL direct-methods routine. The remaining non-hydrogen atoms were located from successive difference Fourier map calculations. The refinement was carried out by using full-matrix least-squares techniques on F². In the final cycles of refinement, all non-hydrogen atoms were assigned anisotropic temperature factors. Methyl and cyclopentadienyl hydrogen atom positions were calculated and allowed to ride on the carbon to which they are bonded, assuming a C-H bond length of 0.95 Å. Hydrogen-atom temperature factors were fixed at 1.10 times the isotropic temperature factor of the carbon atom to which they are bonded. In the case of the terminal and bridging hydride hydrogen atoms, peaks of electron density were located in a Fourier map. While all the hydrogen-atom contributions were calculated, only the hydride atom positions were refined. The final values of R1, wR2, and GOF in the final cycles of the refinements are given in Table 1. The locations of the largest peaks in the final difference Fourier map calculation as well as the magnitude of the residual electron densities in each case were of no chemical significance.

Results and Discussion

The reaction of (Cp')₂ZrCl₂ with excess LiAlH₄ proceeds smoothly at room temperature. While the impure

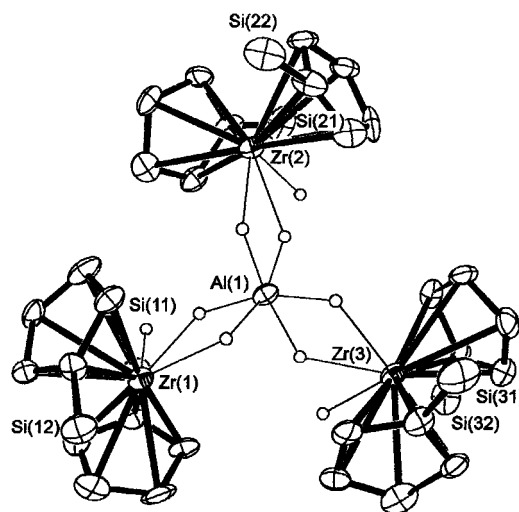


Figure 1. TELP/XP drawing of the Zr₃Al aggregate in the asymmetric unit of **5**; 20% thermal ellipsoids are shown. Al(1)–Zr(1) 3.020(5); Al(1)–Zr(2) 3.033(5); Al(1)–Zr(3) 3.032(5); Zr(1)–Al(1)–Zr(2) 118.7(2); Zr(1)–Al(1)–Zr(3) 113.1(2); Zr(2)–Al(1)–Zr(3) 128.1(2).

residue was thermally unstable, recrystallization of the resulting residue from ether/pentane at –35 °C gives colorless crystals of **5** in 90% yield. The ¹H NMR spectrum of **5** shows singlet resonances at 5.21, 5.37, 5.54, and 5.96 and 0.35 and 0.33 attributable to the cyclopentadienyl and trimethylsilyl protons, respectively. Broad resonances at 2.06, –2.57, and –2.05 arise from hydrides that are bridging Zr and Al and terminal on Zr and Al, respectively. Although the broad resonances infer a dynamic process, the breadth of the signals persisted even upon cooling to –50 °C, thus no structural data could be ascertained. Nonetheless, these data infer aggregation of the Zr hydride with residual alane; the complete structural assignment was not possible as a result of the breadth and relative intensities of these resonances. This prompted the X-ray crystallographic study of **5**.

The results of the structure determination revealed three separate aggregates that cocrystallize in the asymmetric unit of the unit cell. One of these aggregates is formulated as [(Cp')₂ZrH(μ-H)₃Al]. In this Zr₃Al aggregate (Figure 1), three zirconocene units form two hydrogen-atom bridges, each to a central aluminum atom, generating a pseudo-octahedral environment about the aluminum center. Additional terminal hydride atoms reside on each of the zirconium atoms. The two other aggregates in the asymmetric unit are formulated as [(Cp')₂ZrH(μ-H)₂AlH] (Figure 2). In each of these Zr₂Al aggregates two zirconocene fragments are bridged to a central aluminum center by two hydride atoms. Single terminal hydrides reside on each of the two zirconium atoms and the central aluminum center. The geometry about the central Al center is, thus, that of a distorted square-based pyramid. In both the Zr₃Al and Zr₂Al aggregates, the geometry at zirconium is typical of a Cp₂ML₃ fragment. The three hydride atoms lay in the plane bisecting the (Cp')₂Zr fragment. The steric crowding in the Zr₃Al aggregate is reflected in the maximal in-plane H_t–Zr–H_b angle, which has an average of 93.7°, while the corresponding angle in the Zr₂Al aggregates is larger, averaging 109.7°. Similarly, the steric effects are reflected in the H_b–Zr–H_b angles,

(7) *International Tables for X-ray Crystallography*, Knoch Press: Birmingham, England, 1992; Vol. C.

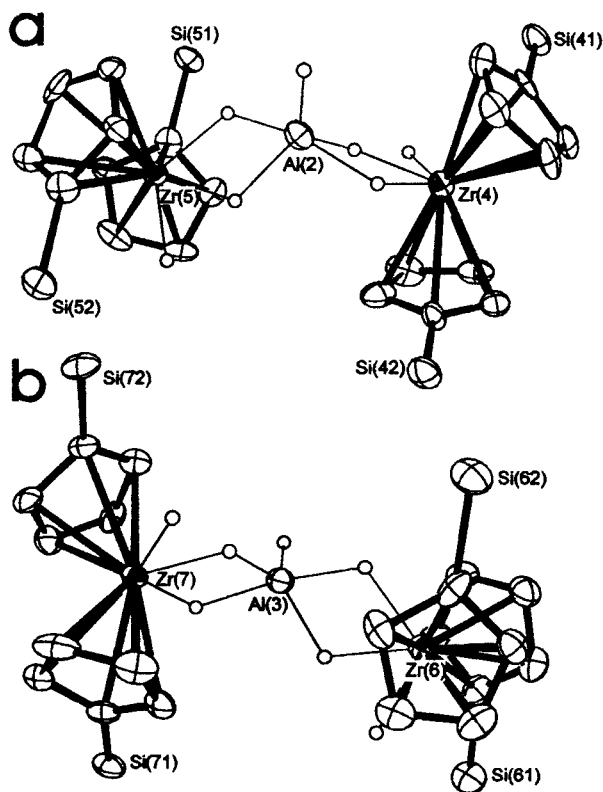


Figure 2. TELP/XP drawing of the two Zr_2Al aggregates (a and b) in the asymmetric unit of **5**; 20% thermal ellipsoids are shown. Al(2)–Zr(5) 2.932(6); Al(2)–Zr(4) 2.943(6); Zr(5)–Al(2)–Zr(4) 132.6(2); Al(3)–Zr(7) 2.936(6); Al(3)–Zr(6) 2.939(6); Zr(7)–Al(3)–Zr(6) 130.9(2).

which average 51.9° in the Zr_3Al aggregate and 60.3° in the Zr_2Al aggregates. In the Zr_3Al aggregate, the

bridging hydrides result in Zr–H_b distances of 1.98 Å while the Al–H_b distances range around 1.52–1.53 Å. The terminal Zr–H bonds are slightly longer, averaging 2.02 Å. In comparison, for the Zr_2Al aggregates, Zr–H_b distances ranging from 1.67 to 1.73 Å and Al–H_b distances of 1.69(1) Å are observed. Terminal Zr–H and Al–H bonds in these Zr_2Al aggregates average 1.68 and 1.65 Å, respectively. The Zr–H and Al–H distances in these Zr_2Al aggregates are similar to those observed for the related complexes $[Cp^*_2ZrH(\mu-H_2)AlH_2]_2$ (**3**) and $Cp_2ZrH(\mu-H_2)AlH_2(L)$ (L = quinuclidine (**1**), NMe₃ (**2**)), although the greater donor ability of Cp' results in longer Zr–H distances.³ In contrast, the Zr_3Al aggregate yields Al–H distances that are more typical of terminal Al–H distances and Zr–H distances that are comparable to those seen in $[Cp^*_2ZrH_3]Li$.⁴ This is consistent with recent computations that suggest that for such zirconocene dihydride–alane adducts, the Zr center acts as a hydride acceptor.³

In conclusion, while the association of zirconocene dihydrides and alane is undoubtedly dynamic in solution, solid-state studies of such species help to identify the variety of modes of aggregation possible. The characterization of **5** confirms the heretofore unprecedented Zr_3Al and Zr_2Al forms of zirconocene dihydride–alane aggregation.

Acknowledgment. This work was supported by the NSERC of Canada.

Supporting Information Available: Tables of crystallographic positional parameters, thermal parameters, and bond distances and angles (33 pages). Ordering information is given on any current masthead page.

OM970849X